Hydraulic fracturing to induce caving: fracture model development and comparison to field data

R.G. Jeffrey
CSIRO Petroleum

A. Settari
Taurus Reservoir Solutions, Ltd.

K.W. Mills
SCT Operations Pty. Ltd.

X. Zhang
CSIRO Petroleum

E. Detournay
University of Minnesota

ABSTRACT: Hydraulic fracturing is used at Moonee Colliery to induce caving as part of the routine operation of this longwall mine. Measurements undertaken to successfully introduce hydraulic fracturing to Moonee and pressure records routinely obtained from each treatment provide a unique opportunity to develop and test a new model of hydraulic fracture growth near a free surface. This paper presents the results of the comparison for several fracture treatments, demonstrating that the model is able to match the treatment data.

1 INTRODUCTION

Moonee Colliery is owned and operated by Coal Operations Australia Limited and the mine is located just south of Newcastle, NSW at Catherine Hill Bay. Mining extracts 3.2 m of the Great Northern seam, leaving, on average, 1.8 m of roof coal and claystone above the seam. This weak roof coal sequence typically caves immediately behind the supports leaving the 30 to 35 m thick conglomerate section bridging the 100 m wide longwall panel.

Hydraulic fracturing is used at Moonee Colliery to grow fractures in the roof rock behind the face. The fractures formed are horizontal and parallel to the base of the conglomerate. Their growth produces caving of the massive conglomerate roof strata at an interval designed to avoid natural caving events.

A new model that accounts for the strong interaction of the hydraulic fracture with the base of the roof conglomerate (a free surface) has been developed. The development and application of the model are the subject of this paper.

2 BACKGROUND

The conglomerate roof has been extensively characterized. Table 1 summarizes measured conglomerate and site properties (Mills et al. 2000). The measured caved profile define a stable arch, which has essentially the same shape whether or not the caving was induced. For the first 50 m behind the face, the arch is a 3D dome-like shape. The caved span curves down both toward the rib line and the face. Further back from the face, the arch maintains an essentially constant shape with a maximum height or 15 m above the base of the conglomerate at the centerline of the panel (see the profile in Fig. 1 labeled "old panel"). Figure 1 contains calculated contours of the vertical stress magnitude on vertical sections across and along the longwall panel.

Table 1: Conglomerate properties.

Property	Value
Depth to seam	160 m
Thickness	30 to 40 m
Compressive strength	35 to 60 MPa
Tensile strength	3.5 to 4.5 MPa
Fracture toughness	0.3 to 1.5 MPa $\sqrt{m}$
Young's modulus	15 to 25,000 MPa
Poisson's ratio	0.2 to 0.3
Maximum in situ stress	8 MPa
Intermediate in situ stress	4 MPa
Minimum in situ stress	4 MPa
Direction of max. stress	N30E grid

3 HYDRAULIC FRACTURING

Hydraulic fractures are placed into the conglomerate from two or three vertical boreholes drilled into the conglomerate from the face. After allowing for the immediate roof thickness, these holes typically penetrate 7 to 9 m into the conglomerate. Once the holes are drilled and an injection hose is grouted in (leaving a 1 m long ungrouted section at the end of the hole), mining resumes. As the face retreats, injection hoses are fed into the goaf behind the supports. If the target roof span is 50 m, the holes are drilled after about 20 m of mining and the fracture treatments are carried out after the full 50 m has been mined.

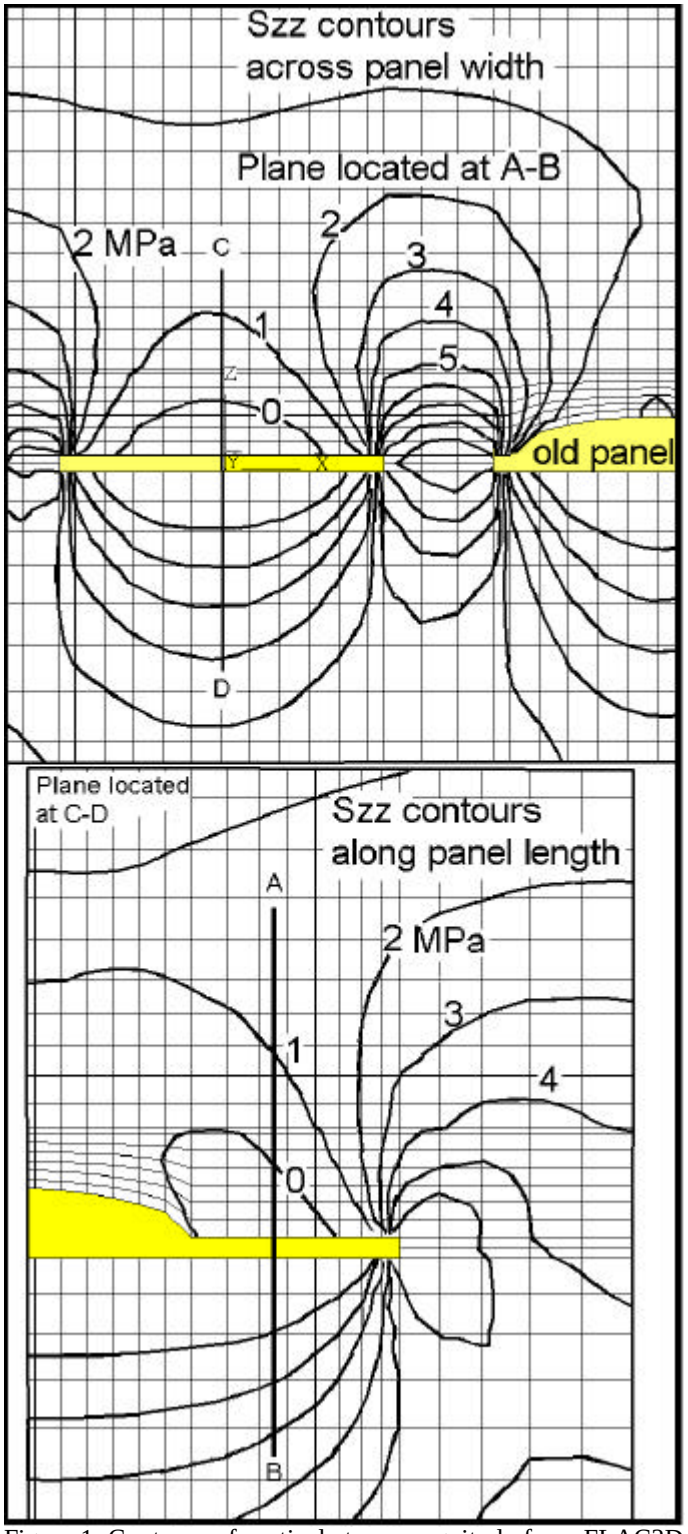

Figure 1: Contours of vertical stress magnitude from FLAC3D on a plane cutting across the panel width (top) and cutting along the length axis (bottom) of the longwall panel.

3.1 *Growth near a free surface*

The effect that the free surface (the base of the conglomerate roof) has on fracture growth depends on the ratio of R/H where R is the fracture radius and H is the distance from the fracture plane to the free surface. As the fracture grows, R/H becomes larger. The opening compliance and the stress intensity factor at the leading edge of the fracture both increase with R/H, which has a significant effect on propagation (Pollard & Holzhausen 1979; Jeffrey et al. 2000; Zhang et al. 2001).

The radial growth model in SIMFRAC (Settari 1988, Jeffrey & Settari 2000) has been modified to account for this increase in opening compliance and stress intensity factor by using an equivalent modulus and K_c approach. The rock modulus is made softer as a function of increasing R/H so that SIMFRAC matches either the fracture volume or the fracture width at the wellbore for an accurate solution of a uniformly pressurized fracture in an elastic half space. This reference solution has been obtained numerically using a recently developed displacement discontinuity model (Zhang et al. 2001). Similarly, the critical stress intensity factor, K_c, is adjusted as described in Appendix B.

The SIMFRAC model has also been modified to accept a negative closure stress, which is a method for taking account of the tensile vertical stresses in the conglomerate at the plane of the fracture (see Fig. 1). Small magnitude tensile vertical stresses exist in the conglomerate between 5 and 15 m above its base.

The model calculates fluid loss from the hydraulic fracture by a 1-D leakoff approximation, which can include wall building and invaded zone coefficients when appropriate. In addition, the model accounts for loss of fluid into a high loss zone (or open borehole) that the fracture may grow into.

The conglomerate roof rock at Moonee has low matrix permeability (on the order or 0.01 md or less) but is cut by two nearly vertical natural fracture joint sets that strike N38E and N55W. The N55W set cuts across the longwall face (which runs at N40W) at a shallow angle and caving events are sometimes associated with the face passing through a fault or dyke running parallel to this joint direction. The average joint spacing for both sets is 3 to 3.5 m (Mawdesley & Trueman 1999) although blocks of conglomerate of 5 m and larger size are often seen in the goaf.

These joints and associated faults provide potential high conductivity pathways for fluid loss. Stress changes during mining are likely to produce small shear and opening movement on these fractures, increasing their conductivity. Fluid loss can, in some cases, dominate the fracture process to such an extent that growth ceases. The option of pumping gels or particulate fluid loss additives is not available because of current limitations on the underground pumping system at Moonee.

Uphole pressure is monitored at Moonee during each treatment via a small-diameter static hose line that is grouted in next to the main injection hose. Monitoring this static pressure in real time provides a reliable method of determining if the fractures are growing or have been stopped by high fluid loss. Growth of the fractures is associated with a continu-

ously decreasing uphole pressure while, if the fracture growth is stopped by high fluid loss (or even leaking grout seals), the uphole pressure becomes constant.

3.2 *Model development and comparison*

The SIMFRAC model has been significantly enhanced to include the effect of the free boundary on fracture width and on stress intensity factors. Entry pressure losses and fluid loss into fractured zones are other features of the model needed to successfully match the treatments described in this paper.

Fracture opening and volume calculated by the half-space DDM model have been used to develop an equivalent modulus, E_e, for SIMFRAC as described in Appendix A. The DDM model is not yet able to simulate either fluid loss or non-Newtonian fluid flow, but solves the elasticity and fracture mechanics problem with a high degree of accuracy, including the displacement on the free surface (see Zhang et al. (2001) for comparisons of the DDM model results to other published half-space results).

Figure 2 compares the opening width profile for a uniformly pressurized fracture with R/H=4.2 as calculated by SIMFRAC and by the DDM model for the case where the fracture opening at the wellbore calculated by SIMFRAC is constrained to match the opening from the DDM model. This modification consists of calculating an equivalent modulus, E_{eW}, as a function of R/H, as described in Appendix A. The opening profile of the same fracture in an infinite elastic space is also shown. The opening width of the fracture becomes highly non-symmetrical for R/H > 2.5 with the lower part displacing farther from the centerline than the upper part. Also, the profile of the width deviates from the (essentially) parabolic shape for a crack in an infinite medium. The approach used in SIMFRAC does not yet account for the correct (DDM) non-symmetric opening effect.

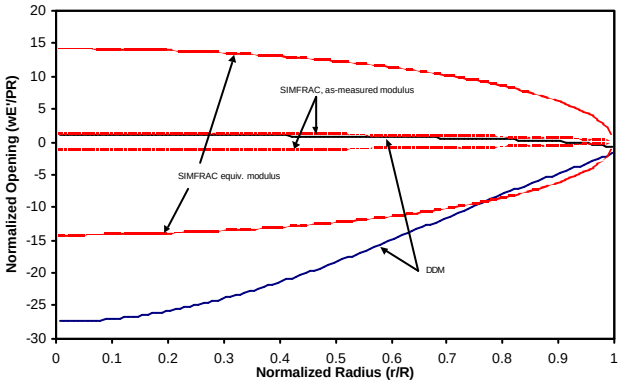

Figure 2: Opening profile of a fracture in an infinite elastic space and near a free surface.

The equivalent modulus for width in SIMFRAC can be made to match the width of the half-space fracture at the wellbore, or the fracture volume. In the first case, the fracture volume is overestimated, while in the second case, the width at the wellbore is underestimated. SIMFRAC pressure and growth rate compare well to the DDM results when the volume matching option is used (see Fig. 3).

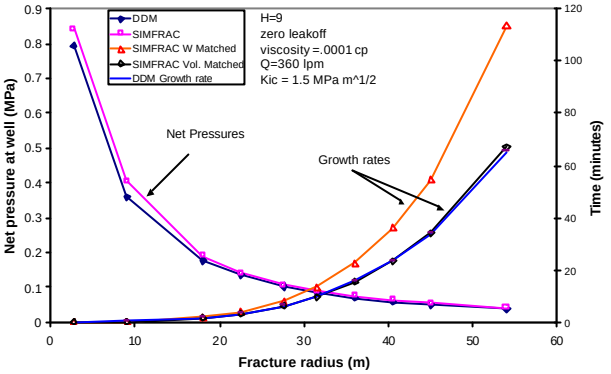

Figure 3: The net pressure and growth rates predicted by the DDM and SIMFRAC models.

The increase in the stress intensity factor because of the presence of a free boundary has been accounted for by changing the critical stress intensity in the inverse ratio. For a plane strain fracture, an analytical solution of Pollard & Holzhausen (1979) provides K_I as a function of L/H. For a radial fracture, reference solutions were obtained by the use of the FRANC2D finite element code (Wawrzynek & Ingraffea 1995) and the DDM code (Zhang et al. 2001). SIMFRAC includes both viscous pressure drop and Kc effects (Jeffrey and Settari 2000), as described in Appendix B. The viscous and toughness dominated propagation regimes have, in recent years, been studied extensively by Detournay (2001) and co-workers. Zhang et al. (2001) discuss this issue and cite several other papers on this topic.

Finally, some of the data shown below exhibits significant entry losses. Because of the small (50 mm diameter) borehole and small fracture width, the entrance area at the crack mouth is initially very small and increases with time. The rate-sensitive pumping pressures at early times (e.g. Fig. 5) reflect these entrance effects. The implementation of entry losses into the model is described in Appendix C.

3.3 *Comparison of model results to field data*

Since being introduced at Moonee in June, 1999, about 60 hydraulic fracture treatments have been carried out. Each treatment is controlled from the surface using a real-time readout of pump pressure, uphole fracture pressure, injection rate and microseismic activity. In a few cases pressure sensors in offset boreholes and roof-to-floor convergence potentiometers were also installed. Three of the more intensively monitored fracture treatments are analyzed below.

3.3.1 *Fracture 2 on Longwall 3*

The second treatment carried out on Longwall 3 included additional monitoring instrumentation to verify the fracture growth behavior and improve our understanding of how the fracture growth was producing caving events. Two vertical boreholes were therefore drilled and completed for injection into the conglomerate. Each hole had a small tube grouted into the hole alongside the main injection line, with its upper end exposed to the fluid pressure at the top of the borehole. In addition, each hole had a roof-to-floor convergence instrument installed between the collar of the hole and the floor directly under it. The injection hole was located about half way across the panel width and the monitoring hole was 15 m further, toward the tailgate side. Figure 4 contains a plan view of the hole layout.

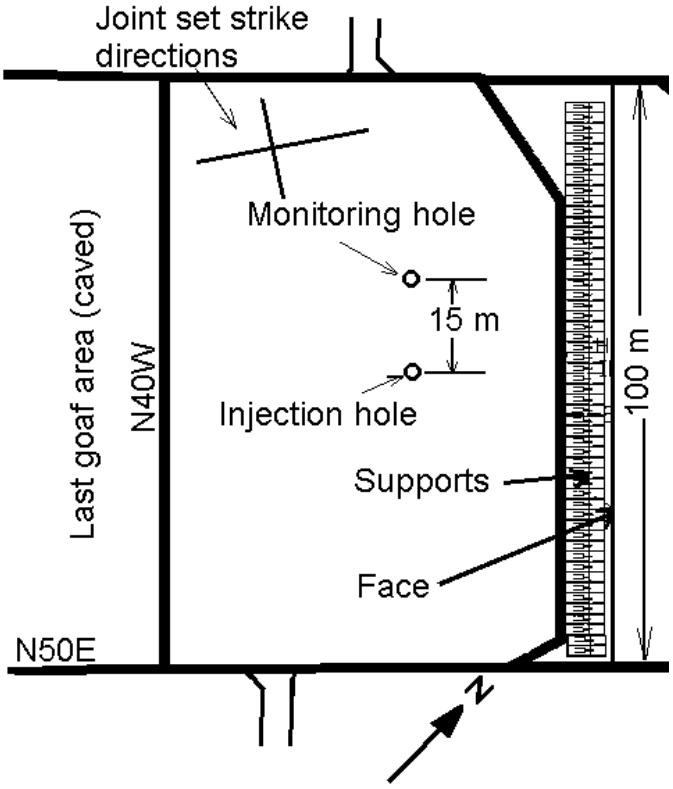

Figure 4: Plan view of hole and face configuration for fracture treatment 2 on Longwall 3.

The pressure declined rapidly after breakdown as water was injected at a constant rate of 360 liters per minute (lpm). Figure 5 provides a summary of the measured pressure and roof to floor convergence. The convergence gage on the injection hole had failed during mining so only convergence at the monitor hole was measured. At three times during the treatment the injection pump was stopped, but water pressure from the supply to the pump was maintained. The water supply pressure was 1.8 MPa and was sufficient to cause a significant flow rate to occur during these shut down periods.

These changes in injection rate provided information about entry pressure losses during different stages of the treatment. In addition, the monitoring hole was intersected by the hydraulic fracture just prior to the second pump stoppage. This intersection provided a direct measure of the fracture size at this point in the treatment and provided a measure of the pressure in the fracture at this location during the rest of the injection.

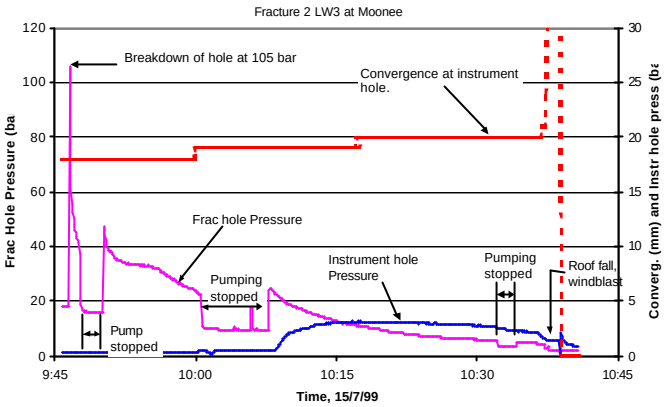

Figure 5: Measured pressure and convergence data during fracture 2 on Longwall 3 at Moonee.

The pressure and growth rate from the model match are superimposed on the collected data in Figure 6.

The match shown was obtained using the parameters listed in Table 2, which are within the range of measured values. The excellent agreement shown required use of all three special modeling features (equivalent modulus to match fracture volume, pseudo-K_c and entry loss at crack entrance).

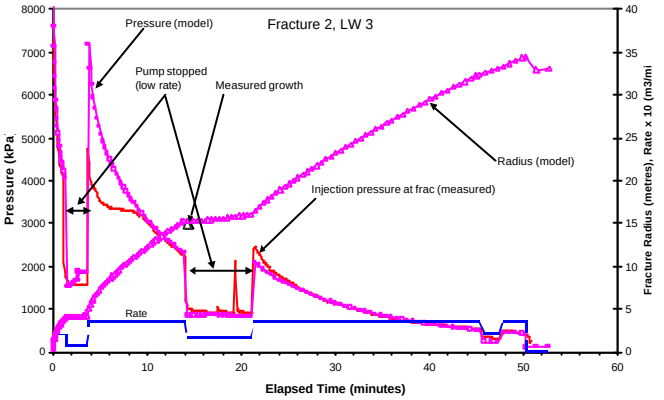

Figure 6: The modeled pressure and growth rate compared to measured data for fracture 2 on LW3.

Table 2: Parameters used to obtain match, F2LW3.

Property	Value
Fracture toughness	1.5 MPa$\sqrt{m}$
Young's modulus	20,000 MPa
Poisson's ratio	0.28
Distance to free surface	9 m
Minimum in situ stress	-0.07 MPa
Pore pressure	50 kPa
Conglomerate porosity	8 percent
Conglomerate permeability	65 md
Total pore compressibility	5.x 10^{-6} kPa $^{-1}$

The measured response for this treatment is representative of treatments that produce roof falls. The uphole pressure continuously decreased throughout the injection period and reached a low value of only

a few hundred kPa just before the fall. Microseismic activity, indicating rock failure and shearing in the roof, began to build before the fall and reached a peak at the time of the fall.

3.3.2 *Fracture 26 on Longwall 3*

The last fracture treatment on Longwall 3 involved two main injection boreholes and three backup injection/monitoring boreholes. A roof-to-floor convergence instrument was installed under each of the two primary injection boreholes. Figure 7 shows the layout of the boreholes and the relative positions of the face and ribs. Holes 1, 2, and 4 were drilled to 7 m while holes 3 and 5 were drilled to only 5 m deep into the conglomerate.

The injection rate was split approximately equally between the two injection holes (1 and 2) by a mechanical flow divider. The actual flow into each hole has been calculated based on the pressure drop measured in the hose running from the output of the flow divider to each hole. During the main treatment, the rates were 257 liters per minute (lpm) into hole 1 and 227 lpm into hole 2.

The breakdown injection cycle was carried out through the flow divider. Hole 1 broke down immediately but hole 2 did not. Consequently, the pressure at hole 2 caused the flow divider to dump part of the injection stream of water via a pressure relief/intensifier circuit. Some of the injected water (estimated as 2,300 litres injected at 92 lpm) passed through the flow divider into hole 1 and extended the fracture. A separate breakdown cycle was then carried out on hole 2, injecting 120 liters at 240 lpm. Modeling of these breakdown cycles indicates that fractures of about 9.6 m and 3.3 m radius would have been created at holes 1 and 2, respectively.

The main treatment was then carried out through the flow divider. The uphole pressures and the measured convergence at the two holes are shown in Figure 8. The pressures recorded at the three monitoring holes (numbers 3, 4, and 5) are also shown.

Simulations were carried out for the injections into holes 1 and 2. Table 3 lists parameters that were common to both simulations. The breakdown cycle pressure data is not shown, but was included in the simulation (Fig. 9) by starting the injection with a 9.6 m radius fracture already present. The pressure measured at hole 2 was matched by using a high fluid loss zone at 16 to 19 m from the hole. Fluid loss increased as the fracture grew through this zone to a maximum loss rate of 104 lpm.

The shape and slope of the convergence curves agrees with deformation at the free surface, arising from fracture growth, up until 10 minutes of injection at hole 1 and 25 to 30 minutes at hole 2 (Fig. 10). After this time the convergence accelerates and becomes concave upward. The additional convergence can arise from unstable fracture growth or roof rock failure adding to the displacement caused by the fracture.

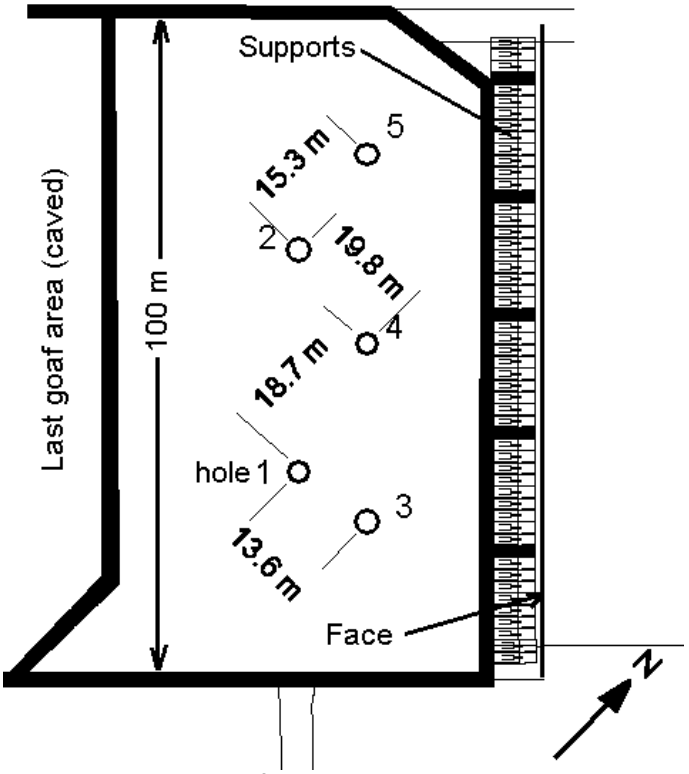

Figure 7: The layout of injection holes (1 & 2) and monitor holes (3, 4, & 5) for fracture treatment 26 on Longwall 3.

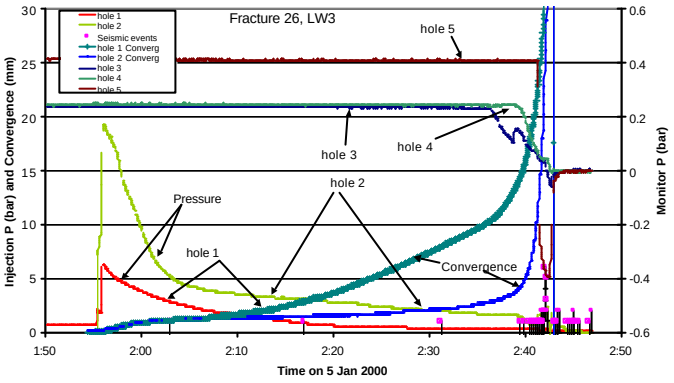

Figure 8: Measured pressure and convergence during fracture 26 on Longwall 3.

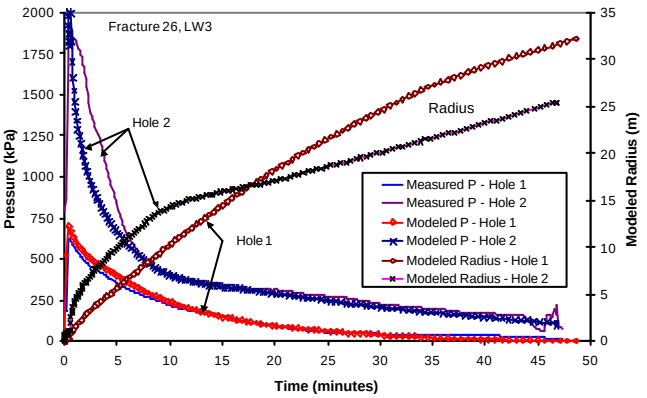

Figure 9: Comparison of model results to measured pressure for fracture 26, LW3.

3.3.3 *Fracture 3 on Longwall 4B*

For this treatment, three injection holes were completed along a narrowed section of the longwall panel. Each hole was initially broken down using 2,000 liters of fluid. The main treatment was then performed into the hole closest to the longwall face (hole 1) while the pressure in hole 2 was monitored. Figure 11 contains a plan view of the longwall panel and hole layout.

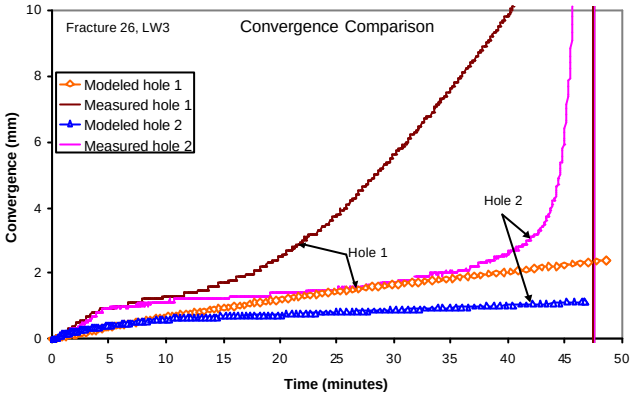

Figure 10: Comparison of modeled roof deflection from fracture to measured roof-to-floor convergence for fracture 26, LW3.

Table 3: Parameters used to obtain match, F26LW3.

Property	Value
Fracture toughness	1.0 MPa$\sqrt{m}$
Young's modulus	20,000 MPa
Poisson's ratio	0.28
Distance to free surface	7 m
Minimum in situ stress	-0.08 MPa
Pore pressure	0 kPa
Conglomerate porosity	8 percent
Conglomerate permeability	30 md
Total pore compressibility	5.x 10^{-6} kPa^{-1}

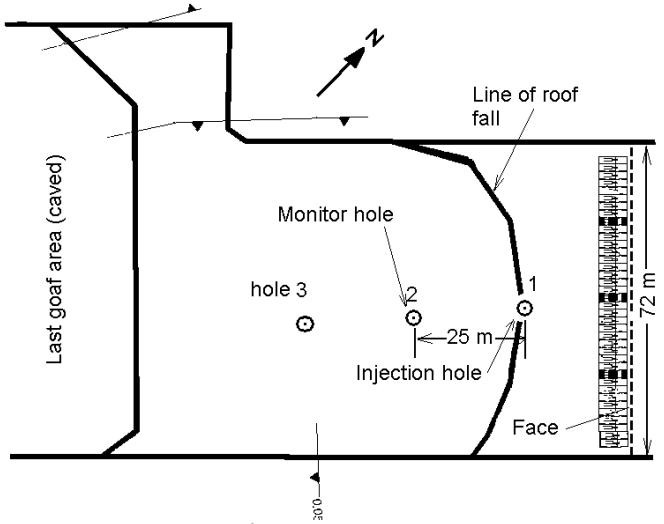

Figure 11: The layout of the injection hole (1) and the monitor hole (2) for fracture treatment 3 on Longwall 4B.

All three holes were drilled to 9.2 m deep into the conglomerate with the top 1 m open. The injection hole was located only 25 m from the face at the time of the treatment. A number of small faults were noted crossing the panel.

Figure 12 contains a plot of the measured uphole injection pressure and the pressure monitored at hole 2. After about 27 minutes of injection into hole 1, a pressure increase occurred at hole 2, indicating the fracture had grown to intersect the already existing fracture at hole 2 (estimated to be about 5 m in radius). This intersection constrains the fracture to be about 20 m in radius at this time in the treatment. The match of the treatment is shown in Figure 13. The parameters used are listed in Table 4.

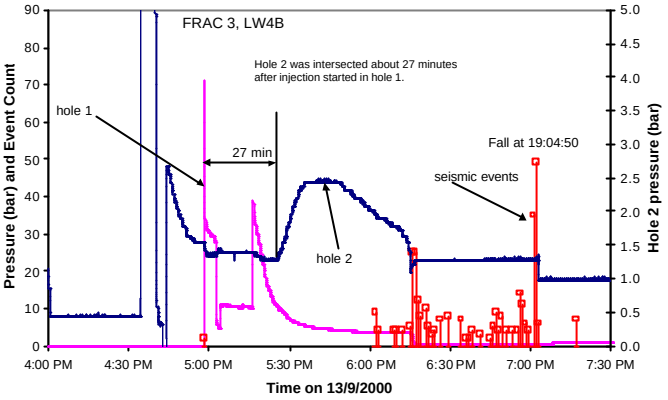

Figure 12: The measured pressure in hole 1 and 2 for fracture 3 on LW4B. The microseismic event frequency is also shown.

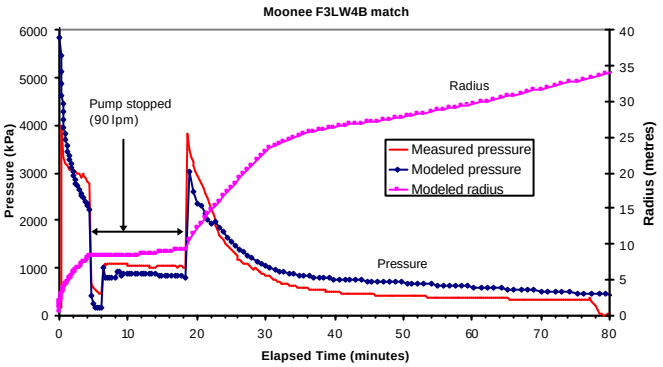

Figure 13: Measured pressure compared to model results for fracture 3 on LW4B.

Table 4: Parameters used to obtain match, F3LW4B.

Property	Value
Fracture toughness	1.2 MPa$\sqrt{m}$
Young's modulus	22,000 MPa
Poisson's ratio	0.28
Distance to free surface	7.8 m
Minimum in situ stress	-0.04 MPa
Pore pressure	0 kPa
Conglomerate porosity	8 percent
Conglomerate permeability	60 md
Total pore compressibility	5 x 10^{-6} kPa^{-1}

Microseismic activity increased sharply at about 6:15 pm and the hole 1 pressure dropped to a low value as the pressure in hole 2 became constant. No roof fall occurred at this time, but pumping was continued until the fall at just after 7 pm.

The fracture model has been used to match the treatment up until the roof movement at 6:15 pm. A high fluid loss zone was included into the model as a way of representing the fracture intersecting a con-

ductive fault or fractured zone. The zone is intersected at 27 to 32 m and the loss rate into this zone is specified to increase to a maximum of 312 lpm. Although the quality of the match is not as good as for fracture 2 on Longwall 3, there is a consistency between the parameters used for the two treatments.

4 DISCUSSION

The measured data, taken together with observations during the treatments and modeling results presented above, suggest broad categories that most treatments can be classified into.

One category is fracture extension followed by arrested growth as a result of the fracture growing into a zone of high fluid loss. When this occurs early in a treatment the fracture radius is limited to be relatively small. Whenever high fluid loss is encountered, the treating pressure becomes constant with time. High fluid loss that stops fracture growth at an early stage produces a relatively high and constant treating pressure (1 MPa or higher).

A second category is fracture growth, associated with a decreasing pressure, continuing throughout the injection. At a fracture radius of about 30 m, the ever increasing effects on K_I from the free surface interaction (added to by the weight of the rock in the delaminated part of the fracture) results in unstable and rapid fracture growth.

The unstable fracture growth may lead to a roof fall event or not, depending on the height of the fracture in the roof as it approaches the face. Fracture growth (which may be unstable during the last few minutes) can extend the fracture to the face, passing over the supports. If the fracture plane over the supports is relatively high in the conglomerate, failure by shear through this thickness of conglomerate cannot occur. The available pump capacity (using water) is not able to overcome fluid loss rates that exist over the large developed fracture surface area. Resuming mining and retreating the face 5 to 7 m has, in many of these cases, resulted in a fall.

The primary factors that control the hydraulic fracture growth in the conglomerate roof have been included into the SIMFRAC model. The growth of the fracture toward the free surface is being addressed by modeling and laboratory studies. The height at which the fractures are initiated is controlled in part by drilling the holes to a certain depth into the conglomerate. However, the fractures may then either initiate as a horizontal fracture at the borehole wall or, because of the hole geometry and the horizontal stress field effects, initiate as a vertical fracture. Vertical fracture initiation will result in the fracture turning to become horizontal as it grows away from the borehole, but the plane of the horizontal fracture may end up higher or lower than the 1 m open hole section of the borehole. On the other hand, stress conditions in the conglomerate below about 5 to 6 m above the free surface start to favor vertical fracture growth, which must be avoided for the treatments to be effective.

5 CONCLUSIONS

Numerical hydraulic fracture models have been developed that account for the strong affect the nearby free surface has on fracture opening compliance and on increased stress intensity factors. Entry pressure losses and leakoff of fluid into pre-existing natural fractures are also important processes that have been included in the modeling.

The SIMFRAC model provides a design tool that can be used to history match treatments already performed and to investigate the effect of changing the treatment details. For example, the benefits of pumping crosslinked gel fluids and particulate fluid loss additives are being investigated as methods to improve the treatment success rate by reducing high fluid loss into naturally fractured zones.

6 ACKNOWLEDGMENTS

We acknowledge the management, staff, and workforce of Coal Operations Australia Ltd. and Moonee Colliery who have supported the work described in this paper. A portion of this work was supported by the Australian Coal Association Research Program. The SIMFRAC model is owned by Duke Engineering & Services and has been developed in collaboration with them.

7 REFERENCES

Abe, H., Mura, T. and Keer, L.M. 1976. Growth Rate of a Penny-shaped Crack in Hydraulic Fracturing of Rocks, *J. Geophys. Res*., Vol. 81, No. 29 (Oct. 1976), pp.5335-5340.

Blevins, R.D. 1992. *Applied Fluid Dynamics Handbook*, Krieger Publishing Co., Malabar, Fla, 1992

Detournay, E. 2001. Propagation Regimes of Fluid-Driven Fractures in Impermeable Rocks. In *Proc. Int. Conf. On Computer Methods and Advances in Geomechanics, Tucson, AZ, 7-12 January* 2001. Rotterdam: A.A. Balkema.

Hayes, P. 2000. Moonee Colliery: Renewing the Economic Viability of a Mine Using Microseismic and Hydraulic Fracturing Techniques in Massive Roof Conditions. Proc. *The 19th Conference on Ground Control in Mining.* August. Morgantown: West Virginia University.

Jeffrey, R.G, & Mills, K.M. 2000. Hydraulic fracturing applied to inducing longwall coal mine goaf falls. Proc. *The Fourth North American Rock Mechanics Symposium.* 31 July – 3 August, 2000. Rotterdam: A.A. Balkema.

Jeffrey, R.G., & Settari, A. 2000. Hydraulic fracture growth through offset pressure-monitoring wells and boreholes. SPE 63031. *2000 SPE Annual Tech. Conf. and Exhib.* Richardson: SPE.

Mawdesley, C., & Trueman, R. 1999. Caving of the conglomerate roof in Newcastle collieries. *JKMRC Mining Research Group report*. Brisbane: U. of Queensland.

Mills, K.M., Jeffrey, R.G., & Jones, D.W. 2000. Successful Application of Hydraulic Fracturing to Control Windblast Hazard. August. *The 19th Conference on Ground Control in Mining*. August. Morgantown: West Virginia University.

Pollard, D.D., & Holzhausen, G. 1979. On The Mechanical Interaction Between a Fluid-Filled Fracture and the Earth's Surface. *Tectonophysics*, 53:27-57.

Settari, A. 1988. Quantitative Analysis of Factors Influencing Vertical and Lateral Fracture Growth. *SPEPE*. August 1988. 310-322.

Wawrzynek, P., & Ingraffea, A. 1995. FRANC2D – A two dimensional crack propagation simulator, User's Guide. Version 2.7, Cornell Fracture Group

Zhang, X., Detournay, E., & Jeffrey, R.G. 2001. Propagation of a Penny-Shaped Hydraulic Fracture Parallel to a Free-Surface, with Application to Inducing Rock Mass Caving for Mining. Proc. *The 38th U.S. Rock Mechanics Symposium*. 7-10 July, 2001. Rotterdam: A.A. Balkema.

8 APPENDICIES

8.1 *Appendix A*

The equivalent modulus E_e for fracture propagating parallel to a free boundary at a distance H, in a media with modulus E, is defined as a modulus, which gives either the same width at the wellbore as the DDM (E_{eW}) or the same fracture volume (E_{eV}). All results were correlated with dimensionless fracture length ξ (ξ=R/H for horizontal, L_f/H for KGD and (H_f/2)/H for PK geometry).

For a radial fracture, the following correlation results from DDM solutions up to ξ=4.2:

$$E_{aW}/E = 1 - 0.0656\xi + 0.3278\xi^2 + 0.0646\xi^3 \quad \text{(A-1)}$$

$$E_{aV}/E = 1 + 0.0356\xi + 0.2654\xi^2 + 0.0232\xi^3 \quad \text{(A-2)}$$

For a KGD or PK fracture, the data of Pollard & Holzhausen was used to obtain:

$$E_{aW}/E = 1 - 0.1985\xi + 0.8502\xi^2 \quad \text{(A-3)}$$

8.2 *Appendix B*

As a planar fracture grows near a free surface, the interaction with the free surface will cause the fracture to turn toward the free surface. If the turning is not allowed, a mode II stress intensity factor, K_{II}, is generated that increases with R/H. In addition, the mode I stress intensity factor, K_I, is also increased. The factor $K_I/K_{Ii} = f(\xi)$ where K_I is the stress intensity in the presence of free boundary and K_{Ii} is in infinite medium, was used to define an equivalent critical stress intensity factor K_{ce} in SIMFRAC as $K_{ce}/K_c = 1/(K_I/K_{Ii})$. The general correlation has a form:

$$K_{ce}/K_c = 1 + [a/(1 + \xi^c)]\,\xi^b \quad \text{(B-1)}$$

The coefficients are:

a = 0.41, b = -1.2, c = 2.0 for radial crack

a = 1.03, b = -1.0, c = 1.18 for KGD crack

The modified K_c is used in equations for the radial geometry presented in Jeffrey & Settari (2000). It should be noted that the definition of K_I used there (Abe et al.1976) is different from the standard definition by a factor of $\sqrt{(2\pi)}$. The effect of fracture turning on the hydraulic fracture process (K_{II}) cannot be represented in SIMFRAC and is being explored using FRANC2D (Wawrzynek & Ingraffea, 1995) and the DDM model.

8.3 *Appendix C*

The entry loss results from the change of direction and crossectional area as fluid flows down a vertical borehole with diameter D_h into a horizontal cylindrical slot of a width W. The problem is simple, yet the exact axisymmetrical geometry has apparently not been studied in the literature. All solutions for the entrance loss are of the form

$$\Delta p = p_1 - p_{2e} = K \tfrac{1}{2} \rho U_2^2 \quad \text{(C-1)}$$

where p_1 and p_{2e} are the pressures upstream and immediately downstream from the entrance, U_2 is the velocity in the entrance and ρ is fluid density. The coefficient K is the "irreversible loss" coefficient and depends on the geometry of the case. In addition, there is a pressure change due to acceleration (kinetic energy changes), which is given by the Bernoulli equation, so the overall equation is

$$p_1 + \tfrac{1}{2} \rho U_1^2 = p_2 + \tfrac{1}{2} \rho U_2^2 + K \tfrac{1}{2} \rho U_2^2 \quad \text{(C-2)}$$

where U_1 is the velocity in the borehole and p_2 is the pressure downstream of the entrance after the flow becomes re-organized. After the fluid enters the fracture, the divergence of the flow causes rapid reduction in velocity from U_2 to U_f in the body of the fracture, and pressure rise from p_2 to p_f. In a diffuser with efficiency E_d this would be accompanied by recovery of pressure by $p_2 - p_f = E_d \tfrac{1}{2}\rho(U_f^2 - U_2^2)$. Therefore there is an additional pressure loss of $(E_d - 1)\tfrac{1}{2}\rho (U_f^2 - U_2^2)$. Since U_f is not known, we have assumed that only the energy recovery up to U_1 can be lost and thus the final equation for losses is:

$$\Delta p_{loss} = p_1 - p_f = K \tfrac{1}{2} \rho U_2^2 + C_d \tfrac{1}{2} \rho (U_2^2 - U_1^2) \quad \text{(C-3)}$$

where K and C_d are input data. Based on data for similar (mostly linear) geometries (e.g., Blevins, 1992), a wide range for K of 0.68 to 2.9 is possible. Fracture will be a poor diffuser; therefore, values of C_d close to 1 are possible. The Moonee data was matched with K in the range of 1-2 and C_d = 1.